

Determination of apparent quantum yield spectra for the formation of biologically labile photoproducts

William L. Miller

Department of Oceanography, Dalhousie University, Halifax B3H 4J1, Canada

Mary Ann Moran¹ and Wade M. Sheldon

Department of Marine Sciences, University of Georgia, Athens, Georgia 30602-3636

Richard G. Zepp and Stephen Opsahl²

Ecosystems Research Division, National Exposure Research Laboratory, U.S. Environmental Protection Agency, Athens, Georgia 30605-2700

Abstract

Quantum yield spectra for the photochemical formation of biologically labile photoproducts from dissolved organic matter (DOM) have not been available previously, although they would greatly facilitate attempts to model photoproduct formation rates across latitudinal, seasonal, and depth-related changes in spectral irradiance. Apparent quantum yield spectra were calculated for two coastal environments from the southeastern United States using postirradiation bacterial respiration as a measure of total labile photoproduct formation and a cutoff filter method to model spectral dependence. As has been the case for previously studied classes of DOM photoproducts (i.e., dissolved inorganic carbon, CO, and H₂O₂), ultraviolet (UV)-B irradiance was significantly more efficient at forming labile photoproducts (i.e., compounds readily assimilated by marine bacterioplankton) than UV-A and visible irradiance. Calculations of DOM photoproduct formation in southeastern U.S. coastal surface waters indicate a formation ratio for biologically labile photoproducts:CO of 13:1. The slope of a natural log plot of the apparent quantum yield spectrum obtained for biologically labile photoproducts was similar to that for CO (0.028 nm⁻¹ vs. 0.034 nm⁻¹). Modeled kinetic rates therefore indicate that the production ratio of these photoproduct classes is approximately maintained despite variations in the solar spectrum that occur with depth in a water column or distance from shore. Application of the apparent quantum yield to coastal regions worldwide predicts an annual formation rate of biologically labile photoproducts in coastal waters of 206×10^{12} g C.

Exposure of marine dissolved organic matter (DOM) to natural sunlight modifies the chemical structure of DOM and produces a suite of organic and inorganic photoproducts that can affect biological productivity (Kieber et al. 1989), oceanic carbon cycling (Mopper et al. 1991; Miller and Zepp 1995), atmospheric flux of CO and CO₂ (Miller and Zepp 1995; Gao and Zepp 1998; Erickson et al. 2000), and many other processes. Although significant progress has been made in identifying DOM photoproducts and documenting

potential effects on biogeochemical processes (Moran and Zepp 1997; Zepp et al. 1998), there are only a few quantitative assessments of DOM photoproduct formation at an ecosystem- or global-level scale (Moran and Zepp 1997; Bertilsson and Tranvik 1998; Johannessen 2000; Mopper and Kieber 2000). This can be attributed, at least in part, to the variation in solar spectral irradiance in both magnitude and quality with latitude, season, stratospheric ozone concentration, water column constituents, water depth, and other factors. Thus, the relationship between photoproduct formation rate and solar spectral irradiance must be understood (or assumed) in order to apply rate measurements over large space and time scales.

The quantitative relationship between photoproduct formation rates and spectral irradiance can be represented by a “quantum yield,” defined as the ratio of the number of photoproduct molecules formed per photon of light absorbed by the compound responsible for product formation. In environmental aquatic photochemistry, where the identity and molar concentration of specific critical chromophores is often not known, the term apparent quantum yield (AQY) is more appropriate and reflects this uncertainty in photochemical mechanisms. Because AQYs are defined for individual wavelengths, they can accommodate differences in light spectra that occur both horizontally and vertically in the ocean. AQYs, when coupled with remotely sensed optical properties of the ocean, can be of use in regional- and global-

¹ Corresponding author.

² National Research Council Research Associate. Present address: Joseph W. Jones Ecological Research Center, Route 2, Box 2324, Newton, Georgia 31770.

Acknowledgments

We thank Penny Kuhn and Lori Ziolkowski for technical support, Cyril Dempsey for assistance obtaining irradiance data in the South Atlantic Bight, Sasha Madronich for providing us with the TUV model, and the University of Georgia Marine Institute on Sapelo Island for hosting the field component of this study. This research was supported by grants from the Office of Naval Research to W.L.M. (N00014-96-1-0408), M.A.M. (N00014-98-1-0530), and R.G.Z. (N00014-98-F-0202). This paper has been reviewed in accordance with the U.S. Environmental Protection Agency’s peer and administrative review policies and approved for publication. Mention of trade names or commercial products does not constitute an endorsement or recommendation for use by the U.S. EPA.

scale assessments of all manner of environmental photochemical processes. For example, regional photochemical production rates for CO and dissolved inorganic carbon (DIC) have been estimated directly from spectra and SeaWiFS imagery-based estimates of ocean color and colored dissolved organic matter (CDOM) distributions (Johannessen 2000).

To this point, AQY spectra have been developed for a number of DOM photoproducts in natural waters, including DIC (Gao and Zepp 1998; Vähälato and Salonen 2000; Johannessen and Miller 2001), carbon monoxide (Valentine and Zepp 1993; Gao and Zepp 1998), carbonyl sulfide (Zepp and Andreae 1994; Weiss et al. 1995), and hydrogen peroxide (Moore et al. 1993; Yocis et al. 2000). These AQY spectra demonstrate consistency across several classes of DOM photoproducts. For example, all exhibit a general exponential decrease in photochemical efficiency with increasing wavelength, with photons in the UV-B region showing more efficient photoproduction (by at least an order of magnitude) than photons in the near visible (Blough 1997; Miller 1999; Moran and Zepp 2000). However, recent detailed studies of apparent quantum yields for DIC from a variety of coastal and open ocean environments suggest that source or chemical composition of marine DOM, or both, can affect the shape and magnitude of AQY spectra, producing variations of sufficient magnitude to influence regional estimates of photoproduct flux (Johannessen and Miller 2001). More information is needed on how quantum yields vary across photoproduct classes and how they are affected by source and composition of DOM.

Biologically labile DOM photoproducts have seldom been the subject of quantum yield studies, despite the fact that they can be a significant source of carbon and energy to microbial food webs and an important pathway for DOM turnover (Miller and Moran 1997; Moran and Zepp 1997; Bertilsson and Tranvik 1998; Mopper and Kieber 2000). The one available action spectrum (i.e., the cross product of AQY spectrum and absorption spectrum) for photochemical formation of formaldehyde from DOM suggests that UV-B wavelengths (280–315 nm) are responsible for the formation of this biologically labile photoproduct, with little or no contribution from UV-A and near visible wavelengths (Kieber et al. 1990). If generally true for all labile DOM photoproducts, AQY spectra for biological substrates would differ considerably from those for carbon gas photoproducts (Zepp et al. 1998) and reactive oxygen species (Blough and Zepp 1995), and global patterns of surface ocean production would therefore vary significantly among categories of DOM photoproducts.

Determination of AQYs for biologically labile DOM photoproducts is complicated by the fact that not all labile photoproducts have yet been identified, and some of the presently uncharacterized molecules do not readily lend themselves to identification (Miller and Moran 1997). Analytical techniques that target known compounds will therefore overlook the potentially large pool of unidentified photoproducts that can affect biological activity. One approach to overcoming this problem is to use a bioassay approach for determination of an apparent quantum yield (i.e., quantifying labile photoproduct formation based on measures of

enhanced bacterial activity), regardless of the chemical structure of the photoproduct. In this study, we take such an approach to determine AQY spectra for labile photoproduct formation for two coastal Georgia environments where previous studies indicated a significant biogeochemical role for biologically labile photoproducts (Miller and Moran 1997; Bushaw-Newton and Moran 1999; Moran et al. 1999).

Materials and methods

Sample collection and irradiation—Apparent quantum yields for biologically labile photoproducts were calculated over the wavelength range of 290–425 nm for DOM collected at two sites on the coast of the southeastern United States in August 1999. The Sapelo Island sample (designated SAP) was collected from a tidal creek draining an extensive *Spartina alterniflora* salt marsh on the western edge of Sapelo Island, Georgia. The Altamaha River sample (ALT) was collected 2 km upstream of the estuary mouth. Both water samples had salinities of 30‰, and initial dissolved organic carbon (DOC) concentrations were 502 (SAP) and 283 μM C (ALT) based on duplicate measures using a Shimadzu TOC-5000 carbon analyzer.

Irradiations were conducted in an Atlas Suntest CPS solar simulator under a 1-kW Xe lamp. Water samples were filtered through ashed GF/F and exhaustively rinsed Poretics 0.2- μm pore size polycarbonate filters and dispensed into 10-cm path length cylindrical quartz cells (~ 30 ml volume, Spectrocell®). Cells were placed in a water-jacketed, custom-built, anodized aluminum block which provided highly reproducible vertical positioning beneath the Xe lamp with temperature controlled at $25.0 \pm 0.1^\circ\text{C}$. Schott long-pass optical glass filters, which blocked radiation at wavelengths shorter than 280 (SAP only), 295, 320, 335, 345, 380, and 425 nm, and cardboard inserts (for dark controls) were positioned between the Xe lamp and sample cells in duplicate directly above each sample cell using an aluminum tray. This arrangement provided duplicate sample irradiation for each of the five or six distinct irradiance spectra without the possibility of “spectral contamination” for adjacent cells. To obtain the specific spectral data appropriate to each cell (required for the AQY calculations described below), the spectral irradiance ($\text{W cm}^{-2} \text{nm}^{-1}$) was measured under each cutoff filter using an Optronic OL754 spectroradiometer fitted with a fiber optic cable (Fig. 1). The spectroradiometer, with fiber optic cable in place, was calibrated twice during the 5 d required to expose all samples using an NBS traceable OptronicOL752-10E irradiance standard. Repetitive scans of the irradiance of our Xe lamp showed less than 1% variation in the irradiance measured at any wavelength. These high-resolution spectral data are important to account for spatial variability within the irradiance field.

Samples were exposed for 6 h at a lamp intensity with a total irradiance (summed from 280 to 400 nm) under the 280-nm cutoff filter of $4.71 \times 10^{-3} \text{ W cm}^{-2}$. This UV irradiance is approximately equivalent to that observed at midafternoon on a clear August day in the southeastern United States. Because of volume constraints with the quartz cells, four separate, sequential irradiations were carried out to ob-

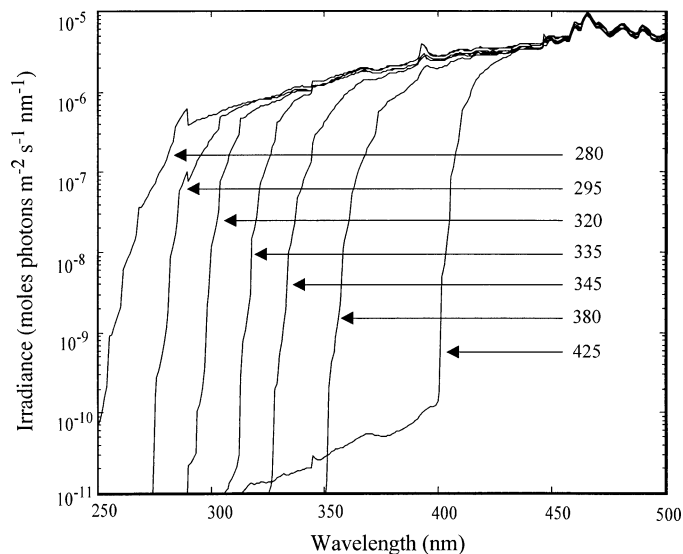


Fig. 1. Spectral irradiance of solar simulator measured under cutoff filters using an Optronics OL754 spectroradiometer fitted with a fiber optic cable.

tain sufficient sample for postirradiation measurements. The first three irradiations were used to establish triplicate bacterial respiration assays. The fourth irradiation was used to measure DOC concentrations, CO photoproduction, and changes in optical properties (absorbance and fluorescence characteristics).

Bacterial respiration assays—To conduct the bacterial respiration assays, postirradiation samples were inoculated with a natural bacterial community from the appropriate (SAP or ALT) site. The bacterial inoculum was prepared by prefiltering 5 L of sample water through a 1.0- μm pore size Poretics polycarbonate filter and trapping bacterial cells that passed the prefilter onto a 0.2- μm pore size Poretics polycarbonate filter. The filter was placed in 300 ml of 0.2- μm filtered sample water and stirred for 10 min to resuspend bacteria. Contents of the two cells irradiated with the same cutoff wavelength were pooled to give 60 ml of irradiated sample. A 600- μl aliquot of the concentrated bacterial inoculum was added [final concentration of 4.0×10^6 cells ml^{-1} (SAP) and 1.7×10^6 cells ml^{-1} (ALT) based on direct epifluorescence counts], along with 6 μl of concentrated inorganic nutrient solution (final concentration of 5 μM NH_4Cl , 5 μM NaNO_3 , and 1 μM NaH_2PO_4) to prevent nutrient limitation of bacterial carbon utilization. Each sample was dispensed into two 27-ml Pyrex flasks outfitted with glass stoppers that had been ground to a point. One flask was immediately fixed with Winkler reagents ($T = 0$) to establish initial dissolved O_2 concentrations. Both flasks were then submerged in a circulating water bath and incubated in the dark at approximately 23°C. After 2 weeks, Winkler reagents were added to the second flask ($T = 2$ weeks). Respiration assays were established in triplicate using irradiated sample water from the first three irradiations (i.e., paired $T = 0$ and 2 weeks flasks were established for each cutoff filter from each of the three irradiations). At the

end of the 2-week incubation, dissolved oxygen concentrations were determined in $T = 0$ and 2 weeks flasks using the precision Winkler method with automatic titration (Mettler DL-21) (Pomeroy et al. 1994).

UV-visible spectra—UV-visible spectra were measured in duplicate for the initial water sample and irradiated samples for each cutoff wavelength. Samples were analyzed over the wavelength range of 250–800 nm on a Shimadzu 160 UV-visible scanning spectrophotometer in 1-cm quartz cuvettes. Absorption coefficients a_λ were calculated as: $a_\lambda = 2.303A_\lambda/\ell$, where A_λ is the measured absorbance at wavelength λ , and ℓ is the path length (m) of the quartz cell.

Spectral slope coefficients were calculated by fitting absorption coefficients to the equation $a_\lambda = a_{\lambda_0} \exp(-S[\lambda - \lambda_0])$, where a_{λ_0} is the absorption coefficient at λ_0 (i.e., 290 nm) and S is the spectral slope coefficient (Zepp and Schlotzhauer 1981; Blough and Green 1995), using a nonlinear least squares method (Sigma Stat, SPSS Inc.). Slopes were calculated over the 290–400 nm spectral region.

CO measurements—The rate of CO photoproduction in each irradiated quartz cell was measured for use in the AQY calculations described below. Immediately following irradiation, 10 ml of sample was removed from the 30-ml total volume with simultaneous injection of CO-free air (made by passing lab air through Schutze reagent, Leco Instruments Inc.) to create a gaseous head space inside the cell. The cells were then shaken vigorously, and a sample of headspace air was withdrawn for analysis of CO concentration using a Trace Analytical Reduction Gas Analyzer. A calibration curve for the instrument was determined using a NIST-traceable CO standard obtained from Scott-Marin Corp. CO concentrations in the irradiated samples were calculated from the headspace analysis using the ratio of the total cell volume to that of the head space, with correction for CO remaining in the aqueous phase using the CO gas–water partition coefficient appropriate for the temperature of equilibration (Wiesenburg and Guinasso 1979).

Determination of photochemical apparent quantum yields—Calculations of the spectral efficiencies for photochemical production of both CO and biologically labile products were based on exactly the same approach, with the single difference being the use of CO photoproduction rates and postirradiation bacterial respiration rates, respectively. A respiratory quotient of 1 was used to convert bacterial O_2 consumption rates to labile photoproduct utilization rates (i.e., each mole of O_2 consumed was assumed to represent utilization of 1 mol of DOC in the form of biologically labile photoproducts). Carbon accumulation in bacterial biomass accounted for a small fraction (<4%) of the total carbon utilization in the 2-week respiration assays and was not considered in the quantum yield calculations.

The apparent quantum yield for each process was determined using the measured kinetic data, pooled from all cells within a given experiment, using the following expression (modified from Balzani and Carassiti 1970).

$$\text{rate} = \int E_{\lambda}(\text{sa}/V)(1 - e^{-a_{\lambda}\ell})(\text{AQY}_{\lambda}) d\lambda \quad (1)$$

Rate is production rate of CO or O₂ (mol L⁻¹ h⁻¹), E_{λ} is the irradiance at wavelength λ (mol m⁻² h⁻¹ nm⁻¹), sa is the irradiated surface area (m²), V is cell volume (L), ℓ is the cell path length (m), a_{λ} is the absorption coefficient (m⁻¹), and AQY_{λ} is the apparent quantum yield, all integrated over the full spectrum of photoactive radiation (280–450 nm).

As described above, the AQY_{λ} used here is different from the traditionally defined photochemical quantum yield, Φ_{λ} , specified as the ratio of the number of moles of product produced or reactant lost to the number of moles of photons absorbed by the reactant at a given wavelength (Braslavsky et al. 1996). In the present study, we do not know the exact identity or molar absorption coefficient of the chromophores driving the photochemistry, the reaction mechanisms, or the specific identity of the carbon compounds that constitute the biologically labile photoproducts resulting in altered oxygen consumption rates. Consequently, we define an “apparent” quantum yield, AQY_{λ} , as shown below.

$$\text{AQY}_{\lambda} = \frac{\text{moles of product (CO or O}_2\text{)}}{\text{moles of photons absorbed by sample}} \quad (2)$$

Using Eq. 1, together with measured spectral irradiance, spectral absorption coefficients, and production rates (CO or O₂), a statistical solution for AQY was obtained with an in-house MATLAB© program based on Rundel’s statistical approach for the optimization of action spectra (Rundel 1983; Cullen and Neale 1997). The mathematical expression used for the fit assumed that the AQY for both CO production and biological response can be described as a function of wavelength using the following exponential equation.

$$\text{AQY}_{\lambda} = e^{-(m_1+m_2[\lambda-290])} \quad (3)$$

m_1 and m_2 are fitting parameters generated by the program and $\lambda = 280\text{--}500$ nm. This assumption of an exponential shape is consistent with previous CO AQY spectra, and our rate data from individual exposures confirmed this general shape for biologically labile photoproduct production. Starting with initial estimates for m_1 and m_2 , the MATLAB program alters these fitting parameters to generate the single AQY spectrum that best minimizes residuals between the measured rate data for all samples from a single exposure and the rates calculated using the photochemical rate Eq. 1.

Fluorescence measurements—Fluorescence properties were determined in duplicate for the initial water sample and irradiated samples for each cutoff wavelength. Samples for fluorescence excitation-emission matrices (EEMS) were diluted with purified water (distilled water that was further treated in a Barnstead NANOpure UV Ultrapure Water System) to the point where A_{350} was <0.02 to minimize inner filtering effects. High-resolution fluorescence matrix scans were performed from 250 to 500 nm excitation (5-nm intervals) and 290 to 650 nm emission (2-nm intervals) using an ISA SPEX Fluorolog 3-12 scanning fluorometer with R928P detector. The instrument was configured for signal ratio mode and dark offset, and both excitation and emission slits

were set to 5-nm band passes. Scans were corrected for instrument configuration according to the manufacturer’s guidelines and Coble et al. (1993) and converted to quinine sulfate equivalents according to Coble et al. (1998). Rayleigh and Raman scatter peaks were eliminated during postprocessing of the data in MATLAB (Release 11). An algorithm was developed to excise scatter peaks (i.e., peak emission $\pm 10\text{--}15$ nm at each excitation wavelength) from the scan data and to replace the excised values using three-dimensional interpolation of the remaining data (Delaunay triangulation method). The interpolated surface was constrained to pass through the nonexcised values so that only data in excised portions were replaced. Following correction and scatter removal, the fluorescence from the NANOpure water diluent was subtracted from each scan and the fluorescence values were multiplied by the dilution factor to calculate the EEMS for the original undiluted sample.

Underwater irradiance measurements—Depth profiles of underwater irradiance were measured using a Satlantic Free Fall OCP-100 profiling instrument. The instrument was equipped with seven OCI-200 downwelling irradiance sensors (325, 340, 380, 412, 443, 490, and 555 nm) and seven OCR-200 upwelling radiance sensors (at matching wavelengths), and tilt angle was measured during deployment. Calibrations indicate that the accuracy of the cosine response of this instrument for irradiance incident within 0–60° of normal is 3%, and within 60–85° of normal is 10%. Downwelling irradiance was also simultaneously measured at these same wavelengths on the ship deck by an OCI-200 sensor. Measurements were logged using Satlantic’s Satview software during a cruise in the South Atlantic Bight on the R/V *Bluefin* on 28 June 1999, and irradiance data were obtained using Satlantic’s ProSoft software. Diffuse attenuation coefficients, $K_d(\lambda)$, were computed from exponential fits to the downwelling irradiance data ($r^2 > 0.98$ in all cases) obtained in the upper part of the water column (where the irradiance was $>10\%$ of the near-surface value) using irradiance data obtained when the tilt was $<5^\circ$. The standard deviation of $K_d(\lambda)$ for six to eight casts at each station was $<10\%$ of the mean at all wavelengths. Plots of $K_d(\lambda)$ versus wavelength were exponential in the UV and blue spectral region ($r^2 > 0.98$). The exponential fits were used to estimate $K_d(\lambda)$ for unmeasured regions of the spectrum that were required for the modeling studies ($r^2 = 0.98$ for 325–442 nm integration).

Modeling studies—To model the depth dependence for photoproduction of biologically labile photoproducts and CO in southeastern U.S. coastal waters, we used the TUV model of Madronich (1993) and Madronich et al. (1998) to simulate the solar spectral irradiance reaching the water surface as a function of latitude, time, total ozone, and other atmospheric parameters. After transforming this irradiance to photon scalar irradiance, downwelling spectral irradiance just under the water surface, $E_d(0, \lambda)$, was computed using Fresnel’s Law to estimate reflective loss as the radiation passes through the air–water interface. The scalar irradiance $E_o(0, \lambda)$ near the water surface was computed using Eq. 4 from the down-

welling irradiance, assuming that upwelling irradiance was comparatively negligible.

$$E_o(0, \lambda) = E_d(0, \lambda)/\bar{\mu}_d \quad (4)$$

$\bar{\mu}_d$, the average near-surface cosine (ratio of depth to mean light path length), was computed using Eq. 5.

$$\bar{\mu}_d^{-1} = f_{dir}(\lambda)\sec \theta + 1.19f_{diff}(\lambda) \quad (5)$$

θ is the angle of refraction of the direct component of sunlight near the water surface, and $f_{dir}(\lambda)$ and $f_{diff}(\lambda)$ are the fractions of solar irradiance that are direct and diffuse, respectively (Zepp and Cline 1977; Gordon 1989; Huot et al. 2000).

The scalar irradiance as a function of depth was computed using Lambert–Beer’s law (Smith and Baker 1978; Gordon 1989) according to Eq. 6.

$$E_o(z, \lambda) = E_o(0, \lambda)e^{-K_d(\lambda)z} \quad (6)$$

$E_o(z, \lambda)$ is the scalar irradiance at depth z and wavelength λ ($\text{mol m}^{-2} \text{ d}^{-1} \text{ nm}^{-1}$) and assuming the diffuse attenuation coefficient for downward irradiance (K_d) is close in value to that for scalar irradiance (Kirk 1994). The rate at a given depth, $\text{rate}(z)$ ($\text{mol L}^{-1} \text{ d}^{-1}$), was computed using Eq. 7.

$$\text{rate}(z) = j \int E_o(z, \lambda)(a_\lambda)(\text{AQY}_\lambda) d\lambda \quad (7)$$

j is a unit conversion factor equal to $0.001 \text{ m}^3 \text{ L}^{-1}$.

To model the photoproduction fluxes of biologically labile photoproducts for the coastal ocean, we used a modified version of the GCSOLAR model. The flux was computed by integrating the cross product of the net downwelling spectral irradiance just under the water surface, $\bar{E}(0, \lambda)$, and the apparent quantum yields (AQY_λ) over the range of photoactive wavelengths (i.e., 280–450 nm; Eq. 8).

$$\text{Flux} = \int \bar{E}(0, \lambda)(\text{AQY}_\lambda) d\lambda \quad (8)$$

We assumed in our calculations that the net downwelling irradiance, $\bar{E}(0, \lambda)$, and the downwelling irradiance, $E_d(0, \lambda)$, were equivalent (Kirk 1994).

Like the TUV model, the GCSOLAR package (version 1.2, 2001) contains a set of routines written in FORTRAN 90 that compute photolysis rates in the aquatic environment as a function of season, latitude, time of day, depth in water bodies, and ozone layer thickness. A more detailed description of the rate equations appear in Zepp and Cline (1977). The present version of GCSOLAR uses equations described by Green et al. (1980) and Baker et al. (1980) to compute spectral irradiance in the UV region (280–390 nm) reaching the water surface. Total ozone averaged over the period from 1979–1992 was used for the computations.

Results

Changes in optical properties during irradiation—Bleaching of chromophoric DOM during irradiation reduced absorbance of the SAP and ALT samples (Table 1). The greatest reduction occurred with the >295 nm cutoff filter

Table 1. Optical properties of SAP and ALT DOM following irradiation using a range of cutoff filters that allowed passage of radiation at wavelengths from >425 to >295 nm. a_{350} and a_{410} are the absorption coefficients at 350 and 410 nm, respectively. Integrated fluorescence is calculated as the volume under the EEMS (250–500 nm excitation, 290–650 nm emission). Values are the mean of two replicate cells, except for SAP < 425 and ALT > 380, for which $n = 1$.

Site	Irradiation range	a_{350} (m^{-1})	a_{410} (m^{-1})	Spectral slope coefficient	Integrated fluorescence ($\text{qsu} \times 10^{-3}$)	Δ Integrated fluorescence (%)
SAP	none	11.2	3.9	0.0168	2,663	0
	>425	10.9	3.6	0.0172	2,532	−5.0
	>380	10.4	3.4	0.0178	2,256	−15.3
	>345	10.0	3.4	0.0181	2,014	−24.4
	>320	9.5	3.4	0.0175	1,782	−33.1
	>295	9.5	3.4	0.0169	1,726	−35.2
	>280	9.6	3.4	0.0163	1,677	−37.0
ALT	none	5.7	2.3	0.0159	1,241	−1.9
	>425	5.5	2.1	0.0164	1,179	−6.8
	>380	5.4	2.1	0.0167	1,081	−14.5
	>345	5.1	2.0	0.0170	1,062	−16.0
	>320	4.8	2.0	0.0165	947	−25.1
	>295	4.8	2.0	0.0158	922	−27.1

(~15% at 350 nm excitation) and the least with the >425 nm filter (~2% at 350 nm) (Fig. 2). Bleaching was most extensive at wavelengths above the cutoff wavelength of the filter but was not confined to this region. For example, samples irradiated under the 425 nm cutoff filter bleached at wavelengths as low as 350 nm, although the greatest losses occurred at wavelengths >400 nm (Fig. 1).

Fluorescence fading (measured as changes in integrated volume under the surface of the EEMS) was more extensive than absorbance fading, with losses ranging from 5.0% (>425 nm filter) to 35.2% (>295 nm filter) for the SAP sample and 6.8% (>425 nm filter) to 27.1% (>295 nm filter) for the ALT sample (Table 1).

Apparent quantum yield for biologically labile photoproducts—Using cumulative bacterial oxygen consumption during the 2-week postirradiation incubation as an index of labile photoproduct formation (i.e., respiratory activity per absorbed photon), the photoproduction rates for biologically labile photoproducts were determined. These rates increased with decreasing cutoff wavelength of the filter for both the SAP and ALT samples (Fig. 3).

Equations for biologically labile photoproduct AQYs as a function of wavelength were similar for the two coastal sites (Fig. 4). Parameters m_1 and m_2 in Eq. 3 were 5.633 and 0.0298, respectively, for the Sapelo water sample ($r^2 = 0.984$) and 5.486 and 0.0273, respectively, for the Altamaha sample ($r^2 = 0.975$).

Apparent quantum yield for carbon monoxide—Rates of carbon monoxide photoproduction during the irradiations increased with decreasing cutoff wavelength of the filter for the SAP and ALT samples (Fig. 3), and the apparent quan-

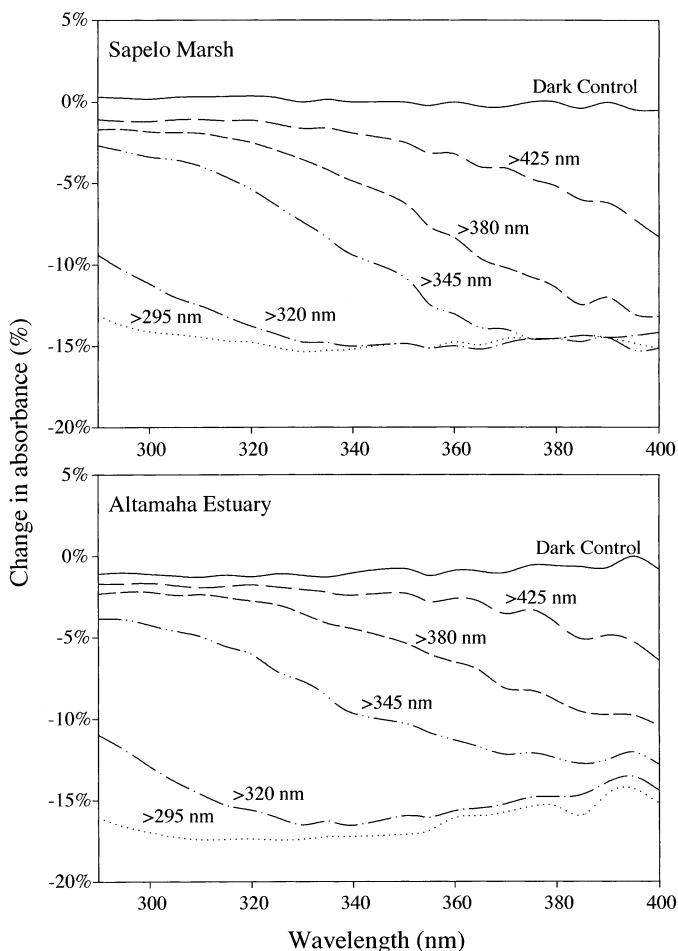


Fig. 2. Percent change in absorbance following irradiation of water from a Sapelo marsh and the Altamaha River estuary using a range of cutoff filters that allow passage of radiation at wavelengths of >425 nm to >295 nm and in dark (nonirradiated) controls.

tum yields were generally 10–20 times lower than the rates for labile photoproduct formation (Fig. 4). Using Eq. 1 to describe the quantum yield spectra, computed parameters for the SAP sample were $m_1 = 8.001$ and $m_2 = 0.037$ ($r^2 = 0.992$) and for the ALT sample were $m_1 = 8.004$ and $m_2 = 0.059$ ($r^2 = 0.867$) (Fig. 4). The slightly lower confidence levels for the ALT sample reflect the fact that fewer points were used in the calculation since CO concentrations were below detection limits in all samples exposed only to wavelengths ≥ 345 nm.

Discussion

Calculating quantum yield spectra by the cutoff filter method—Quantum yield spectra for photoproducts are most commonly determined by irradiation with monochromatic light, using a series of individual wavelengths to construct a plot of AQY_λ versus wavelength (e.g., Valentine and Zepp 1993; Yocis et al. 2000). An alternative approach that has been employed for at least a decade in photobiological studies makes use of cutoff filters that add back increasing re-

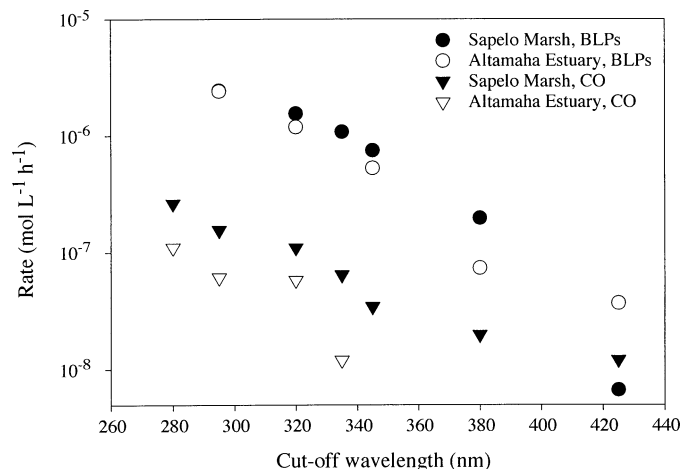


Fig. 3. Comparison of the rates of photoproduction of biologically available photoproducts (BLPs) and carbon monoxide (CO) in water samples from a salt marsh on Sapelo Island and from the Altamaha River estuary. The samples were irradiated using a range of cutoff filters that allow passage of radiation at wavelengths from >425 to >295 nm. Rates of formation of BLPs were computed using cumulative bacterial oxygen consumption in inoculated samples during subsequent 2-week incubations (i.e., respiratory activity per absorbed photon).

gions of the solar spectrum, in conjunction with a mathematical fitting function, to calculate quantum yield spectra (Rundel 1983; Cullen and Neale 1997; Neale 2000). Although this method has not typically been used in photochemical studies, the cutoff filter approach is far less time consuming than the monochromatic approach and is more easily performed in the field. This allows AQY determinations to be completed on freshly collected samples, an important consideration when addressing carbon bioavailability. Furthermore, it has the potential to capture interaction

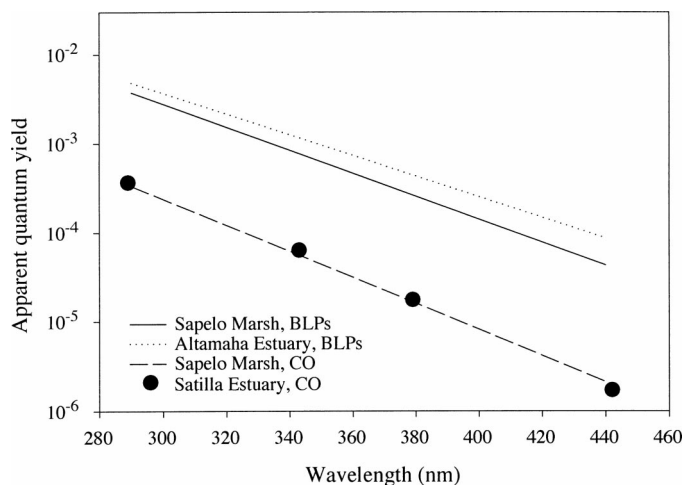


Fig. 4. Comparison of apparent quantum yield spectra for the photoproduction of biologically labile photoproducts and carbon monoxide in SAP and ALT samples. Apparent quantum yields at discreet wavelengths for direct photoproduction of CO calculated previously for the nearby Satilla Estuary are shown for comparison (Gao and Zepp 1998).

effects between wavelengths that are present simultaneously in natural sunlight (Cullen and Neale 1994). This long-pass cutoff filter approach has been used successfully on seawater samples in the determination of AQY spectra for dissolved inorganic carbon (DIC) (Johannessen and Miller 2001) and CO (Ziolkowski 2000). Similarly, Vähälato and Salonen (2000) used the radiation filtering effects of natural lake waters during in situ incubations in place of defined cutoff filters to produce different spectral irradiation for use in calculating AQY spectra for DIC photoproduction, and Osburn et al. (2001) used cutoff filters to calculate spectral weighting functions for DOM bleaching.

The AQY spectra that have been determined previously for the photoproduction of CO from natural waters using monochromatic radiation (Valentine and Zepp 1993; Gao and Zepp 1998) provide a comparative data set for the AQY spectrum for CO calculated here by the cutoff filter method. These previous AQY spectra for CO agree very well with the SAP AQY for CO, particularly in the case of the nearby Satilla Estuary (Fig. 4) (Gao and Zepp 1998). Vähälato et al. (2000) and Ziolkowski (2000) have likewise obtained nearly identical AQY spectra in direct comparisons of the traditional monochromatic irradiation approach and the multispectral approach.

Comparison of quantum yield spectra among classes of DOM photoproducts—Kieber et al. (1989) presented an action spectrum for the photoproduction of formaldehyde, a commonly identified biologically labile photoproduct in both marine and freshwater environments. The two biologically labile photoproduct AQY spectra calculated here, however, are the first to incorporate all photoproducts that can be used as substrates by bacterioplankton, regardless of chemical structure. These quantum yields show a greater contribution of UV-A and visible wavelengths to biologically labile photoproduct formation relative to the Kieber et al. (1989) formaldehyde action spectrum. Indeed, the spectral dependence of our AQYs is quite similar to that observed for other well-studied classes of DOM photoproducts (i.e., CO, DIC, and H₂O₂) from a variety of marine and freshwater environments, as evidenced by the similarity in slopes (Fig. 4). Comparable spectral responses may indicate a similar source or mechanism of formation for many classes of DOM photoproducts. Similar slopes for AQY spectra, and therefore similar patterns in surface ocean production among categories of DOM photoproducts, would greatly simplify efforts to model photoproduct formation on regional or global scales.

However, there is also recent evidence that AQY spectra for DOM photoproducts vary spatially, and that DOM source or light exposure history can influence formation rates. For example, Johannessen and Miller (2001) found that the slopes of log-linearized AQY spectra for DIC photoproduction from coastal and inshore samples were steeper than slopes of spectra from water samples collected in the open ocean or from inshore samples experimentally photobleached prior to AQY determination. Such differences in the slope of AQY spectra, together with generally greater UV absorbance in coastal waters, predict that rates of DIC formation will drop off much more rapidly with depth in coastal environments than in the open ocean. Although these depth

effects might be of little consequence for long-term geochemical cycling of DOM, they could be of considerable importance for atmosphere exchangeable products and for photochemical reactions in highly stratified systems.

The two coastal ecosystems studied here have consistently shown net positive effects of photoreactions on DOM lability (Miller and Moran 1997; Moran et al. 1999; Bushaw-Newton and Moran 1999), likely because of strong influences from vascular plant-derived organic matter from coastal marshes and rivers (Moran et al. 2000). However, the issue of determining AQY spectra for biologically labile photoproducts over broader geographic scales is complicated by recent studies showing negative effects of DOM irradiation on subsequent bacterial activity in some aquatic ecosystems (Benner and Biddanda 1998; Tranvik and Kokalj 1998; Obernosterer et al. 1999). Although quantum yield information for environments exhibiting a net negative effect will be required before the spectral dependence of biologically labile photoproduct formation can be fully disentangled, the AQY spectra presented here are likely to be generally applicable for terrestrially influenced coastal systems.

Depth-dependent formation of biologically labile photoproducts—Because the fraction of the water column that experiences full sunlight conditions is typically small, the ecological relevance of DOM photoreactions must be considered on a depth-integrated basis. Quantum yield spectra allow location-specific, depth-integrated calculations because they provide the wavelength-specific rate information necessary to account for the varying characteristics of solar radiation due to seasonal and latitudinal effects and for the differential penetration of solar irradiance into the water column (Moran and Zepp 2000).

We calculated depth-specific formation rates of two classes of DOM photoproducts for a region of the southeastern U.S. continental shelf (32°N latitude) in midsummer using the AQY spectra for biologically available photoproducts and CO calculated in this study (Fig. 4). In surface waters of the continental shelf, conversion of DOM to biologically labile photoproducts was calculated to be about 13-fold greater than to CO (Fig. 5). The ratio between the two classes of photoproducts changed only slightly with water depth (15:1 at 2 m deep and 16:1 at 4 m deep), as expected, considering the similar shape of the AQY spectra for both classes of photoproducts (Fig. 4). Thus, although absolute rates of photoproduct formation decreased in proportion to the diminution of available radiation (i.e., approximately 6-fold at 2 m deep and 20-fold at 4 m deep), the relative contribution of the two major classes of photoproducts was not substantially different. The calculations show that UV-A radiation is primarily responsible for inducing formation of biologically labile photoproducts (Fig. 5).

At the water surface, where irradiance is maximal, the model estimates daily production of biologically labile photoproducts of 3.2 $\mu\text{mol C L}^{-1} \text{d}^{-1}$ (Fig. 5). Moran and Zepp (1997) previously predicted photoproduction of 0.9 $\mu\text{mol C L}^{-1} \text{d}^{-1}$ of biologically labile photoproducts in surface waters of the southeastern U.S. shelf under similar irradiance conditions but used an approach based on summing identified photoproducts for which published rate measurements were

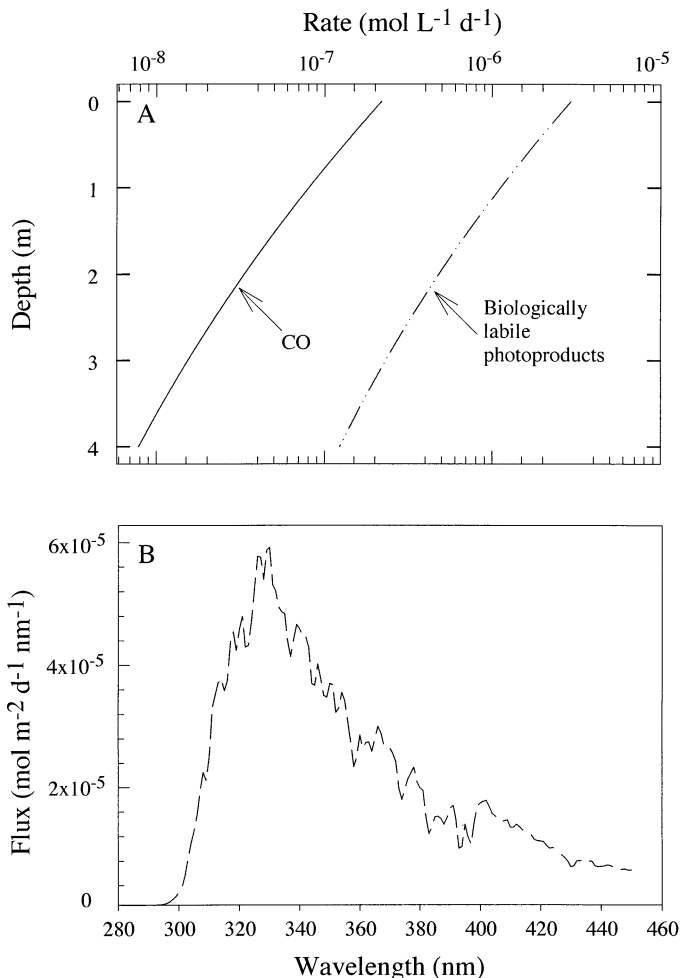


Fig. 5. (A) Rates of photochemical formation of biologically labile photoproducts as a function of depth on the southeastern U.S. shelf. Formation rates were computed based on quantum yield spectra from this study, a diffuse attenuation coefficient, $K_d(\lambda)$ (measured in the South Atlantic Bight in June 1999; 31°43.43'N, 80°38.83'W), and irradiance typical of midday on a cloudless summer day (28 June) in the southeastern United States. Rates of photochemical formation of CO are shown for comparison. (B) Wavelength dependence of biologically labile photoproduct flux (same conditions as for A).

available (i.e., acetaldehyde, acetate, formaldehyde, formate, glyoxal, glyoxylate, levulinate, propanal, and pyruvate). Thus, chemically uncharacterized DOM photoproducts, not included in the previous rate estimate of Moran and Zepp (1997), are incorporated into this new estimate.

Coastal ocean calculations—We now speculate on the potential global production of biologically labile photoproducts in the coastal ocean if the AQY spectrum calculated here for southeastern U.S. waters is typical for coastal regions worldwide. For this exercise, we assume that incident sunlight (290–450 nm) is absorbed by DOM that can produce biologically labile photoproducts with the same efficiency as SAP DOM. Although it is not yet possible to assess the validity of this assumption for biologically labile photoproducts,

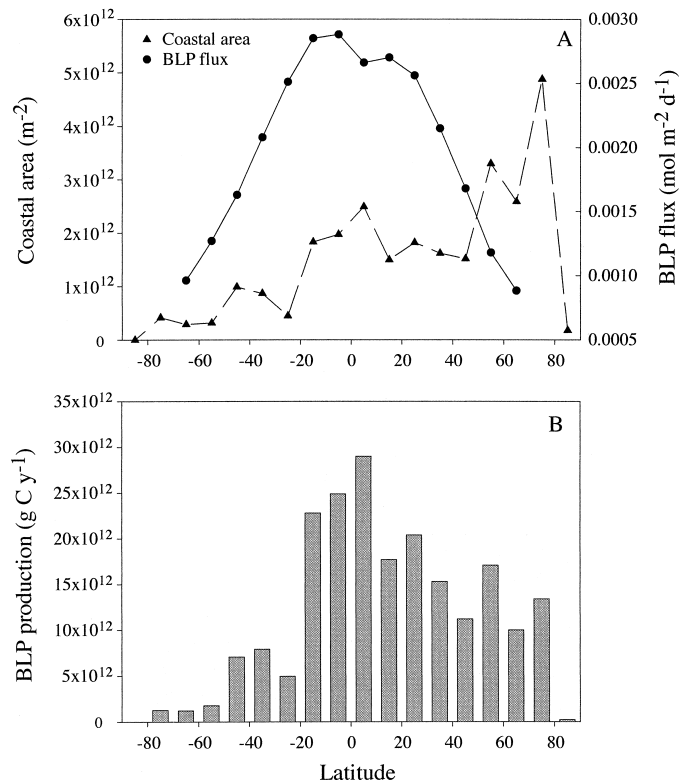


Fig. 6. (A) Cloud-corrected latitudinal distribution of coastal ocean and average daily formation rates (m^{-2} of ocean surface) of biologically labile photoproducts by 10° -latitude bands calculated using the SAP quantum yield spectrum. (B) Annual formation of biologically labile photoproducts by 10° -latitude bands calculated from the cross product of data in the top panel.

comparisons of AQY spectra for CO (for which a larger data base is available) indicate that the SAP CO spectrum is within a factor of two of the median AQY for a variety of terrestrial systems (Valentine and Zepp 1993; Miller and Zepp 1995; Bourbonniere et al. 1997; Moran and Zepp 1997; Gao and Zepp 1998). Calculations of average daily depth-integrated photoproduct formation rates (i.e., $\text{mol m}^{-2} \text{d}^{-1}$) were made for 10° -latitude bands using the GCSOLAR model between 65°S and 65°N (Fig. 6A), with corrections for cloud cover based on Frederick and Lubin (1988). Results suggest that depth-integrated formation rates of biologically labile photoproducts in the coastal ocean are highest in the tropics and subtropics, where annual solar flux is greatest, and lowest at high latitudes (Fig. 6A). Annual production of biologically labile photoproducts by 10° -latitude bands was estimated from the cross product of the calculated depth-integrated fluxes (extrapolating cloud cover data to 85° latitude) and the latitudinal distribution of the coastal ocean, as calculated from data in Levitus (1982) (assuming $27.1 \times 10^6 \text{ km}^2$ of coastal ocean; Menard and Smith 1966) (Fig. 6A). Most biologically labile photoproduct formation is predicted to occur in the Northern Hemisphere, with substantial contributions from high-latitude coastal regions (Fig. 6B). The estimated annual production of biologically labile photoproducts from coastal regions worldwide is $206 \times 10^{12} \text{ g C}$, a value that approximately corresponds to the annual

global input of riverine DOM (220×10^{12} g C; Hedges 1992). However, this calculation overestimates photoproduction if sunlight is absorbed by DOM (either terrestrial or marine) with a lower efficiency of photoproduct formation. Nonetheless, formation of biologically labile photoproducts has the potential to be a major sink of terrestrial DOM exported to the sea. This is consistent with previous estimates of potential CDOM consumption in coastal oceans by direct photooxidation (Andrews et al. 2000).

Formation of biologically labile photoproducts in the open ocean cannot be calculated from our data because the AQY spectrum is based on terrestrially influenced DOM and because recent research suggests that surface water DOM in the open ocean might not be a source of biologically labile photoproducts, at least in a net sense (Benner and Biddanda 1999; Obernosterer et al. 1999). If biologically labile photoproduct formation in oceanic surface waters is indeed negligible, then turnover of marine DOM via biologically labile photoproducts can be only a small fraction of the total DOM turnover in the ocean (i.e., less than 1% assuming annual turnover of $>50 \times 10^{15}$ g C; Hedges 1992). For biologically labile photoproduct formation to be significant globally, it would have to be demonstrated that formation rates equivalent to those estimated here also apply to tropical and subtropical open ocean water.

References

- ANDREWS, S. S., S. CARON, AND O. C. ZAFARIOU. 2000. Photochemical oxygen consumption in maine waters: A major sink for colored dissolved organic matter? *Limnol. Oceanogr.* **45**: 1783–1792.
- BAKER, K. A., R. C. SMITH, AND A. E. S. GREEN. 1980. Middle ultraviolet radiation reaching the ocean surface. *Photochem. Photobiol.* **32**: 367–374.
- BALZANI, V., AND V. CARASSITI. 1970. *Photochemistry of coordination compounds*. Academic Press.
- BENNER, R., AND B. BIDDANDA. 1998. Photochemical transformations of surface and deep marine dissolved organic matter: Effects on bacterial growth. *Limnol. Oceanogr.* **43**: 1373–1378.
- BERTILSSON, S., AND L. J. TRANVIK. 1998. Photochemically produced carboxylic acids as substrates for freshwater bacterioplankton. *Limnol. Oceanogr.* **43**: 885–895.
- BLOUGH, N. V. 1997. Photochemistry in the sea-surface microlayer, p. 383–424. *In* P. Liss & R. Duce [eds.], *The sea surface and global change*. Cambridge Univ. Press.
- , AND S. A. GREEN. 1995. Spectroscopic characterization and remote sensing of nonliving organic matter, p. 23–45. *In* R. G. Zepp and C. Sonntag [eds.], *Role of non-living organic matter in the earth's carbon cycle*. Wiley.
- BLOUGH, N. V., AND R. G. ZEPP. 1995. Reactive oxygen species in natural waters, p. 280–333. *In* C. S. Foote et al. [eds.], *Active oxygen: Reactive oxygen species in chemistry*. Chapman and Hall.
- BOURBONNIERE, R. A., W. L. MILLER, AND R. G. ZEPP. 1997. Distribution, flux, and photochemical production of carbon monoxide in a boreal beaver impoundment. *J. Geophys. Res.-Atmos.* **102**: 29321–29329.
- BRASLAVSKY, S. E., K. N. HOUK, AND J. W. VERHOEVEN. 1996. *Glossary of terms used in photochemistry*. 2nd ed. International Union of Pure and Applied Chemistry. Amsterdam.
- BUSHAW-NEWTON, K., AND M. A. MORAN. 1999. Photochemical formation of biologically available nitrogen from dissolved humic substances in coastal marine environments. *Aquat. Microb. Ecol.* **18**: 285–292.
- COBLE, P., C. E. DEL CASTILLO, AND B. AVRIL. 1998. Distribution and optical properties of CDOM in the Arabian Sea during the 1995 southwest monsoon. *Deep-Sea Res., Part II*: **45**: 2195–2223.
- , C. A. SCHULTZ, AND K. MOPPER. 1993. Fluorescence contouring analysis of DOC intercalibration experiment samples: A comparison of techniques. *Mar. Chem.* **41**: 173–178.
- CULLEN, J. J., AND P. J. NEALE. 1994. Ultraviolet radiation, ozone depletion, and marine photosynthesis. *Photosynth. Res.* **39**: 303–320.
- , AND ———. 1997. Biological weighting functions for describing the effects of ultraviolet radiation on aquatic systems, p. 97–118. *In* D. P. Hader [ed.], *Effects of ozone depletions on aquatic ecosystems*. R.G. Landes Company.
- ERICKSON, D., R. G. ZEPP, AND E. ATLAS. 2000. Ozone depletion and the air-sea exchange of greenhouse and chemically reactive trace gases. *Chemosphere-Global Change Sci.* **2**: 137–149.
- FREDERICK, J. E., AND D. LUBIN. 1988. The budget of biologically active ultraviolet radiation in the earth-atmosphere system. *J. Geophys. Res.* **93**: 3825–3832.
- GAO, H., AND R. G. ZEPP. 1998. Factors influencing photoreactions of dissolved organic matter in a coastal river of the southeastern United States. *Environ. Sci. Technol.* **32**: 2940–2946.
- GORDON, H. R. 1989. Can the Lambert-Beer law be applied to the diffuse attenuation coefficient of ocean water? *Limnol. Oceanogr.* **34**: 1389–1409.
- GREEN, A. E. S., K. CROSS, AND L. A. SMITH. 1980. Improved analytic characterization of ultraviolet light. *Photochem Photobiol.* **31**: 59–65.
- HEDGES, J. I. 1992. Global biogeochemical cycles: progress and problems. *Mar. Chem.* **39**: 67–93.
- HUOT, Y., W. H. JEFFREY, R. F. DAVIS, AND J. J. CULLEN. 2000. Damage to DNA in bacterioplankton: A model of damage by ultraviolet radiation and its repair as influenced by vertical mixing. *Photochem. Photobiol.* **72**: 62–74.
- JOHANNESSEN, S. C. 2000. A photochemical sink for dissolved organic carbon in the ocean. Ph.D. dissertation, Dalhousie University. May 2000.
- , AND W. L. MILLER. 2001. Quantum yield for the photochemical production of dissolved inorganic carbon in the ocean. *Mar. Chem.* In press.
- KIEBER, D. J., J. MCDANIEL, AND K. MOPPER. 1989. Photochemical source of biological substrates in sea water: implications for carbon cycling. *Nature* **341**: 637–639.
- KIEBER, R. J., X. ZHOU, AND K. MOPPER. 1990. Formation of carbonyl compounds from UV-induced photodegradation of humic substances in natural waters: fate of riverine carbon in the sea. *Limnol. Oceanogr.* **35**: 1503–1515.
- KIRK, J. T. O. 1994. *Light and photosynthesis in aquatic ecosystems*. Cambridge Press. 509 p.
- LEVITUS, S. 1982. *Climatological atlas of the world ocean*. NOAA Professional Paper 13, DOC/NOAA, U.S. Government Printing Office, 173 p.
- MADRONICH, S. 1993. The atmosphere and UV-B radiation at ground level, p. 1–39. *In* L. O. Björn, and A. R. Young [eds.], *Environmental UV Photobiology*. Plenum Press.
- , R. L. MCKENZIE, L. O. BJÖRN, AND M. M. CALDWELL. 1998. Changes in biologically active ultraviolet radiation reaching the Earth's surface, p. 1–27. *In* *Environmental effects of ozone depletion: 1998 Assessment*. United Nations Environmental Programme.
- MENARD, H. W. AND S. M. SMITH. 1966. Hypsometry of ocean basin provinces. *J. Geophys. Res.* **71**: 4305–4325.
- MILLER, W. L. 1999. Effects of UV radiation on aquatic humus:

- Photochemical principles and experimental considerations, p. 125–143. *In* D. O. Hessen and L. Tranvik [eds.], Aquatic humic substances. Springer-Verlag.
- , AND M. A. MORAN. 1997. Interaction of photochemical and microbial processes in the degradation of refractory dissolved organic matter from a coastal marine environment. *Limnol. Oceanogr.* **42**: 1317–1324.
- , AND R. G. ZEPP. 1995. Photochemical production of dissolved inorganic carbon from terrestrial organic matter: significance to the oceanic organic carbon cycle. *Geophys. Res. Lett.* **22**: 417–420.
- MOORE, C. A., C. T. FARMER, AND R. G. ZIKA. 1993. Influence of the Orinoco River on hydrogen-peroxide distribution and production in the eastern Caribbean. *J. Geophys. Res.* **98**: 2289–2298.
- MOPPER, K., AND D. J. KIEBER. 2000. Marine photochemistry and its impact on carbon cycling, p. 101–129. *In* S. de Mora, S. Demers, and M. Vernet [eds.], The effects of UV radiation in the marine environment. Cambridge Univ. Press.
- , X. ZHOU, R. J. KIEBER, D. J. KIEBER, R. J. SIKORSKI, AND R. D. JONES. 1991. Photochemical degradation of dissolved organic carbon and its impact on the oceanic carbon cycle. *Nature* **353**: 60–62.
- MORAN, M. A., AND R. G. ZEPP. 1997. Role of photoreactions in the formation of biologically labile compounds from dissolved organic matter. *Limnol. Oceanogr.* **42**: 1307–1316.
- , AND ———. 2000. UV radiation effects on microbes and microbial processes, p. 201–228. *In* D. L. Kirchman [ed.], Microbial ecology of the oceans. Wiley.
- , W. M. SHELDON, AND J. E. SHELDON. 1999. Biodegradation of riverine dissolved organic carbon in five estuaries of the southeastern United States. *Estuaries* **22**: 55–64.
- , ———, AND R. G. ZEPP. 2000. Carbon loss and optical property changes during long-term photochemical and biological degradation of estuarine dissolved organic matter. *Limnol. Oceanogr.* **45**: 1254–1264.
- NEALE, P. J. 2000. Spectral weighting functions for quantifying effects of UV solar radiation in marine ecosystems, p. 72–100. *In* S. de Mora, S. Demers, and M. Vernet [eds.], The effects of UV radiation in the marine environment. Cambridge Univ. Press.
- OBERNOSTERER, I., B. REITNER, AND G. J. HERNDL. 1999. Contrasting effects of solar radiation on dissolved organic matter and its bioavailability to marine bacterioplankton. *Limnol. Oceanogr.* **44**: 1645–1654.
- OSBURN, C. L., H. E. ZAGARESE, D. P. MORRIS, B. R. HARGREAVES, AND W. E. CRAVERO. 2001. Calculation of spectral weighting functions for the solar photobleaching of chromophoric dissolved organic matter in temperate lakes. *Limnol. Oceanogr.* **46**: 1455–1467.
- POMEROY, L. R., J. E. SHELDON, AND W. M. SHELDON. 1994. Changes in bacterial numbers and leucine assimilation during estimations of microbial respiratory rates in seawater by the precision Winkler method. *Appl. Environ. Microbiol.* **60**: 328–332.
- RUNDEL, R. D. 1983. Action spectra and estimation of biological effective UV radiation. *Physiol. Plant* **58**: 360–366.
- SMITH, R. C., AND K. S. BAKER. 1978. Optical classification of natural waters. *Limnol. Oceanogr.* **23**: 260–267.
- TRANVIK, L., AND S. KOKALJ. 1998. Decreased biodegradability of algal DOC due to interactive effects of UV radiation and humic matter. *Aquat. Microb. Ecol.* **14**: 301–307.
- VÄHÄTALO, A. V., M. S.-SALONEN, P. TAALAS, K. SALONEN. 2000. Spectrum of the quantum yield for photochemical mineralization of dissolved organic carbon in a humic lake. *Limnol. Oceanogr.* **45**: 664–676.
- VALENTINE, R. L., AND R. G. ZEPP. 1993. Formation of carbon monoxide from the photodegradation of terrestrial dissolved organic carbon in natural waters. *Environ. Sci. Technol.* **27**: 409–412.
- WEISS, P. S., S. S. ANDREWS, J. E. JOHNSON, AND O. C. ZAFIRIOU. 1995. Photoproduction of carbonyl sulfide in South Pacific ocean waters as a function of irradiation wavelength. *Geophys. Res. Lett.* **22**: 215–218.
- WIESENBERG, D. A. AND N. L. GUINASSO. 1979. Equilibrium solubilities of methane, carbon monoxide, and hydrogen in water and sea water. *J. Chem. Eng. Data* **24**: 356–360.
- YOCIS, B. H., D. J. KIEBER, AND K. MOPPER. 2000. Photochemical production of hydrogen peroxide in Antarctic waters. *Deep-Sea Res. Pt. 1-Oceanog. Res. Pap.* **47**: 1077–1099.
- ZEPP, R. G., AND M. O. ANDREAE. 1994. Factors affecting the photochemical production of carbonyl sulfide in sea water. *Geophys. Res. Lett.* **21**: 2810–2816.
- , AND D. M. CLINE. 1977. Rates of direct photolysis in the aquatic environment. *Environ. Sci. Technol.* **11**: 359–366.
- , AND P. F. SCHLOTZHAUER. 1981. Comparison of photochemical behavior of various humic substances in water: III. Spectroscopic properties of humic substances. *Chemosphere* **10**: 479–486.
- , T. V. CALLAGHAN, AND D. J. ERICKSON. 1998. Effects of enhanced solar ultraviolet radiation on biogeochemical cycles. *J. Photochem. Photobiol. B: Biology* **46**: 69–82.
- ZIOLKOWSKI, L. A. 2000. Marine photochemical production of carbon monoxide. M.Sc. Thesis. Dalhousie University. 121 pp.

Received: 27 July 2001

Accepted: 16 November 2001

Amended: 10 December 2001